Atomic layer deposition and properties of mixed Ta_2O_5 and ZrO_2 films

Kaupo Kukli, Marianna Kemell, Marko Vehkamäki, Mikko J. Heikkilä, Kenichiro Mizohata, Kristjan Kalam, Mikko Ritala, Markku Leskelä, Ivan Kundrata, and Karol Fröhlich

Citation: AIP Advances **7**, 025001 (2017); doi: 10.1063/1.4975928

View online: http://dx.doi.org/10.1063/1.4975928

View Table of Contents: http://aip.scitation.org/toc/adv/7/2

Published by the American Institute of Physics

Atomic layer deposition and properties of mixed Ta_2O_5 and ZrO_2 films

Kaupo Kukli,[1,2,a] Marianna Kemell,[1] Marko Vehkamäki,[1] Mikko J. Heikkilä,[1] Kenichiro Mizohata,[3] Kristjan Kalam,[2] Mikko Ritala,[1] Markku Leskelä,[1] Ivan Kundrata,[4] and Karol Fröhlich[4]

[1]*Department of Chemistry, University of Helsinki, P.O. Box 55, FI-00014 Helsinki, Finland*
[2]*Institute of Physics, University of Tartu, W. Ostwald 1, 50411 Tartu, Estonia*
[3]*Accelerator Laboratory, Department of Physics, University of Helsinki, P.O. Box 43 (A.I. Virtasen aukio 1), FI-00014 Helsinki, Finland*
[4]*Institute of Electrical Engineering, Slovak Academy of Sciences, Dúbravská Cesta 9, 841 04 Bratislava, Slovakia*

(Received 28 December 2016; accepted 27 January 2017; published online 6 February 2017)

Thin solid films consisting of ZrO_2 and Ta_2O_5 were grown by atomic layer deposition at 300 °C. Ta_2O_5 films doped with ZrO_2, $TaZr_{2.75}O_8$ ternary phase, or ZrO_2 doped with Ta_2O_5 were grown to thickness and composition depending on the number and ratio of alternating ZrO_2 and Ta_2O_5 deposition cycles. All the films grown exhibited resistive switching characteristics between TiN and Pt electrodes, expressed by repetitive current-voltage loops. The most reliable windows between high and low resistive states were observed in Ta_2O_5 films mixed with relatively low amounts of ZrO_2, providing Zr to Ta cation ratio of 0.2. [http://dx.doi.org/10.1063/1.4975928]

INTRODUCTION

Artificially combined and structured metal oxides have gained interest as materials exhibiting interesting and advanced physical and chemical properties. Herewith Ta_2O_5 and ZrO_2 composites mixed within a variable range of tantalum to zirconium cation ratios have been studied as materials of possible interest towards several applications. Ta_2O_5-ZrO_2 mixtures produced by the sol-gel technique have been characterized in terms of their structure, surface acidity, and catalytic properties.[1] Tantala doped zirconia has been of interest due to its thermomechanical behavior.[2] Corrosion resistance of structurally and mechanically stable, mostly orthorhombic, ZrO_2–Ta_2O_5,[3,4] or ZrO_2-Nb_2O_5-Ta_2O_5[5,6] pellets and powders have been examined and described.

Electronic and structural properties of tantalum-doped monoclinic ZrO_2 have both been characterized theoretically.[7] Zirconia nanocrystals have been stabilized in the tetragonal phase of ZrO_2 by tantalum doping.[8] Phase diagrams for the Ta_2O_5-ZrO_2 system, including ternary zirconate phases,[9] have been described. Ta_2O_5-ZrO_2 composite polycrystalline powders have been described as materials possessing dielectric permittivity values up to 50.[10] Dielectric properties of $Ta_2Zr_6O_{17}$ films obtained by composition-combinatorial approach through the sol-gel technique were characterized.[11] In zirconium doped tantalum oxide films, sputtered on nitride electrodes, leakage current densities lower than those in undoped tantalum oxide, were measured.[12] Sputtered Ta_2O_5-ZrO_2 high-k gate dielectric films have been studied for potential applications in metal-oxide-semiconductor (MOS) devices.[13,14] Zr-doped TaO_x high dielectric constant (high-k) films were deposited on silicon wafer pre-covered with tantalum nitride to hinder the formation of the SiO_x interface layer during the subsequent high-temperature annealing step.[15] A large variety of metal oxides has exhibited resistive switching behavior.[16–22] Tantalum oxide has, however, been one of the most prominent candidate material in the field of memristor technology. Mostly sputtered, but also atomic layer deposited tantalum

[a]Corresponding author, e-mails: kaupo.kukli@helsinki.fi, kaupo.kukli@ut.ee

oxide films with variable stoichiometry have been investigated as materials suitable for the application in resistance switching memory cell capacitors.[17,19,20,23–27] TiN/Ta_2O_5/Ta,[28,29] Pt/TaO_x/HfN_x,[30] Al/Cu/Ti/TaO_x/W,[31] Pd/(TiO_2)Ta_2O_{5-x}/TaO_y/Pd[27] and Pt/TaO_x/Ta[26] resistive switching memory cells have been fabricated. Concentration of defects in the Ta_2O_5 layers and, in particular, the existence and tunability of the content of oxygen vacancies has been considered and studied as an important factor affecting the memristive performance of TaO_x-based cells.[32,33] The switching, as observed, has been dependent on the choice of electrode materials in direct contact to the oxide layer. Highly reactive metals, such as Ti and Zr, have produced low yields for switchable TaO_x based devices, whereas Ni and noble metals (Pd, Pt, Au) did not create sufficiently oxygen vacancies at the top metal–oxide interface via chemical reactions resulting in unipolar switching dominated by thermal effects.[34] Stable bipolar resistive switching has been observed in structures containing one electrode acting as a basis for cation-oxygen exchange (reactive metals) and non-reacting (noble) metals as the second electrode. Regarding the useful thickness of the oxide based memristive devices, one can apply TaO_x layers with thickness below 1-2 nm, still exhibiting reliable resistive switching properties.[29]

ZrO_2 has also been frequently described as a thin film material exhibiting resistive switching. The effect was observed when deposited, e. g., between Pt and TiN electrodes either in the form of undoped ZrO_2 alone[35] or together with HfO_2.[36] Furthermore, resistive switching has been described in ZrO_2 films containing implanted Zr^+ in Au/Cr/Zr^+-ZrO_2/n^+-Si,[37] indium-tin-oxide/ZrO_2/Ag,[38] Ag/ZrO_2/Ag,[39] Ti/ZrO_2/Pt,[40–42] Cu/ZrO_2/Pt,[44] and Ni/ZrO_2/TaN[45] stacks. ZrO_2 has therewith been deposited by sputtering,[42,43,45] spin coating,[39] electron beam evaporation[44,46,47] and laser ablation.[40,41] It is to be noted that resistive switching has been observed and evaluated in amorphous ZrO_2 films as well.[42] It has also been found that embedding an amorphous ZrO_2 layer in Pt/ZrO_2/TiO_2/Pt structure can result in excellent bipolar switch in comparison with Pt/TiO_2/Pt device.[48] In a few cases, ZrO_2 layers have artificially formed as defective host materials, prone to filamentary switching, after distribution of metallic (i.e. not intentionally oxidized) implants in the oxide, exemplified by Cu/ZrO_2:Cu/Pt,[47] Ti/ZrO_2 with embedded Mo layer/Pt,[49] and Cu/ZrO_2:Ti/Pt,[50] and Cu/TiO_x–ZrO_2/Pt[50] based ReRAM stacks. In the latter case, 20 nm thick ZrO_2 films were deposited by electron beam evaporation, followed by atomic layer deposition of TiO_2 layer.

It may occur challenging to keep strict control over the defect density and the suitable degree of stoichiometry in metal oxides subjected to resistance switching. For instance, artificially defective TaO_x/Ta_2O_5 films have been created by implanting oxygen ions into pre-sputtered 50 nm thick Ta films.[51] Controlled fabrication of resistive switching stacks by atomic layer deposition has been considered as a complicated process, due to the difficulties related to feasible formation of medium rich of oxygen vacancies, in which the filament forms, as well as an O vacancy deficient layers to control the filament rupture.[52] However, there are recent works devoted to atomic layer deposition of memristive TaO_x based switches built on TiN/Ta_2O_5/Ta/TaN stacks with 1-4 nm thick tantalum oxide films.[29] In another study, 7 nm thick Ta_2O_5 layers in TiN/Ta_2O_5/TiN and TiN/Ta_2O_5/Al_2O_3/TiN stacks were grown by ALD from $Ta(OC_2H_5)_5$, and H_2O.[53]

ALD of zirconium oxide doped tantalum oxide films with the purpose to use the material in transistor gate dielectric films has been claimed.[54] Ta_2O_5 thin films have been grown in a water-free ALD process from $Ta(OC_2H_5)_5$ and $TaCl_5$.[55,56] ZrO_2-Ta_2O_5 nanolaminates with improved dielectric characteristics were grown by atomic layer deposition using $Ta(OC_2H_5)_5$, $ZrCl_4$ and H_2O as precursors.[57,58] Enhanced dielectric constant was also measured in ZrO_2-Ta_2O_5 nanolaminates grown by ALD and heat treated after the deposition.[59] However, in the latter study the precursors used were not reported. ZrO_2 films were grown earlier by ALD from $ZrCl_4$ and O_3.[60] It seems that mixed tantalum zirconium oxide films have not yet been grown in water-free ALD process from $Ta(OC_2H_5)_5$ and $ZrCl_4$. However, ALD of zirconium doped tantalum oxide films with the purpose to use the material in transistor gate dielectric has been claimed,[54] whereby the films were grown using alternate cycling of metal precursors $Ta(OC_2H_5)_5$, $TaCl_5$, ZrI_4 (and/or $ZrCl_4$), and H_2O or H_2O_2 as oxygen precursors. Kärkkänen *et al.*[61] have investigated the ALD of ZrO_2 thin films from $Zr[N(CH_3)(C_2H_5)]_4$ and O_3, and studied their resistive switching behavior.

In this study, thin solid films of mixed Ta_2O_5 and ZrO_2 layers were grown by ALD from $Ta(OC_2H_5)_5$ and $ZrCl_4$ as metal precursors. O_3 has optionally been applied as an oxygen source. The oxide films were, alternatively, also grown in direct reactions between halide and alkoxide

precursors along with the so-called water-free hydrolysis route. The study was aimed at the evaluation of the effect of relative content of both cations on the resulting film structure and resistive switching characteristics.

EXPERIMENTAL DETAILS

Ta_2O_5-ZrO_2 films were grown in a flow-type hot-wall ALD reactor F120 (ASM Microchemistry, Ltd.)[62] at a substrate temperature of 300 °C. Zirconium tetrachloride, $ZrCl_4$ (Aldrich, 99.99 %), and tantalum pentaethoxide, $Ta(OC_2H_5)_5$ (Strem Chemicals, 99.9 %), further also denoted as $Ta(OEt)_5$, were used as zirconium and tantalum precursors, respectively. Nitrogen, N_2, was applied as the carrier and purging gas. $ZrCl_4$ and $Ta(OC_2H_5)_5$ were evaporated at 170–185 and 95 °C, respectively, from open boats inside the reactor and transported to the substrates by inert gas valving of the carrier gas flow. Ozone, O_3, used as an additional oxygen precursor, was produced in a Wedeco Ozomatic Modular 4 HC ozone generator from oxygen (99.999%, Linde Gas). The estimated ozone flow rate from the generator during the ozone pulsing was about 220 sccm, while the carrier gas flow rate in the ALD reactor was kept at 400 sccm.

The films were grown via alternate exposure of the substrate surface to either sequential $ZrCl_4$ and $Ta(OC_2H_5)_5$ flows separated by purge periods, or to sequential $ZrCl_4$, $Ta(OC_2H_5)_5$, and O_3 flows separated by purge periods. For example, and further in this paper, the cycle sequencing written as 750 × 0.5-0.5-1.0-0.5 s, TaOEt-p.-$ZrCl_4$-p., will denote 750 ALD cycles, each consisting of 0.5 s long $Ta(OC_2H_5)_5$ pulse, 0.5 s long purge, 1 s long $ZrCl_4$ pulse, and 0.5 s long purge. Analogously, the cycle sequencing written as 100 × [6 × 0.5-0.5-1.0-0.5 s, TaOEt-p.-O_3-p. + 1 × 0.5-0.5-1.5-0.5 s, $ZrCl_4$-p.-O_3-p.] + 6 × 0.5-0.5-1.0-0.5 s, TaOEt-p.-O_3-p. denotes 100 Ta_2O_5-ZrO_2 supercycles, each consisting of 6 ALD cycles for Ta_2O_5 constituent layers grown with 0.5 s $Ta(OC_2H_5)_5$ pulse, 0.5 s purge, 1.0 s O_3 pulse, and 0.5 s purge, and 1 ALD cycle for ZrO_2 constituent layers grown with 0.5 s $Ta(OC_2H_5)_5$ pulse, 0.5 s purge, 1.5 s O_3 pulse, and 0.5 s purge. These 6 Ta_2O_5-ZrO_2 supercycles were followed by 6 ALD cycles for Ta_2O_5, closing the stack of the layers, and making the film symmetrical from electrode to electrode in terms of the chemical composition. The growth cycles applied and some essential characteristics of selected films grown in this study are given in Table I.

The substrates were cut as 5 cm × 5 cm pieces out of undoped Si(100) covered with a 1.5–2.0 nm thick wet chemically grown SiO_2. Selected samples were annealed at 900 °C in N_2 flow for 30 min. Also conducting substrates were used, based on (100) silicon with resistivity 0.014–0.020 Ω·cm, i.e., boron-doped to concentration up to 5×10^{18} –1×10^{19}/cm^3, and coated with 10 nm thick chemical vapor deposited titanium nitride layer. The films were grown to thicknesses ranging from 1 to 100 nm, in order to make the structural and compositional measurements more convenient. Spectroscopic ellipsometer model GES5-E, equipped with a 75 W xenon lamp as a light source emitting a continuous spectrum ranging from ultraviolet to infrared (185 – 2000 nm), was used for the evaluation of the films thicknesses and refractive indexes, The incident light was focused with a microspot with dimensions 365 × 270 μm under 75° incidence angle. In addition, the thicknesses of the films were determined from reflectance spectra measured within a wavelength range of 380–1100 nm using a Hitachi U2000 spectrophotometer and applying a fitting method developed by Ylilammi and Ranta-aho.[63] Grazing incidence X-ray diffractometry (GIXRD) was performed using a PANalytical X'Pert PRO X-ray diffractometer with Cu Kα source at the incidence angle of 1°. Specimens for transmission electron microscopy (TEM) were prepared with the lift-out method[64] in a FEI Quanta 3D 200i focused ion beam (FIB)-scanning electron microscope (SEM), i.e., FIB-SEM dual beam microscope. Bright-field TEM images were taken with a FEI Tecnai F-20 microscope operated at 200 kV.

Energy dispersive X-ray spectrometry (EDX) was applied for the measurements of the zirconium to tantalum atomic ratio, and also for the estimation of the film thicknesses, using a Hitachi S-4800 scanning electron microscope (SEM) equipped with an Oxford INCA 350 EDX spectrometer. The EDX spectra were measured at 30 keV. The beam current and spectrometer gain were determined from a calibration measurement under the same beam conditions. The film thicknesses and ratios of the different elements were calculated from the k ratios of Zr, Ta, and Cl Kα X-ray lines measured with the calibrated beam. The calculations were done with a GMRFILM program,[65]

TABLE I. Sequences of the growth cycles, thickness variations, refractive indexes, Zr:Ta atomic ratios by EDX and contents of constituting elements by ToF-ERDA for Ta_2O_5:ZrO_2 films as-deposited at 300 °C from $Ta(OC_2H_5)_5$ (TaOEt), $ZrCl_4$, and O_3. Precursor pulse lengths are indicated within the cycle sequences. All the precursor pulses were separated by 0.5 s long purge times.

Growth cycle sequences	thickness	refractive index	Zr:Ta	Zr, Ta, and Cl at. %
40 × [15 × 0.5/1.5 s, TaOEt/O_3 + 1 × 0.5/0.5/1.5 s, TaOEt/$ZrCl_4$/O_3] + 15 × 0.5/1.5 s, TaOEt/O_3	27-35 nm	2.202 ± 0.001	<0.2	
160 × [3 × 0.5/1.5 s, TaOEt/O_3 + 1 × 0.5/0.5/1.5 s, TaOEt/$ZrCl_4$/O_3] + 10 × 0.5/1.5 s, TaOEt/O_3	32-40 nm	2.213 ± 0.006	0.2	
250 × [5 × 0.5/1.0 s, TaOEt/O_3 + 1 × 0.5/1.0/1.5 s, TaOEt/$ZrCl_4$/O_3] + 5 × 0.5/1.0 s, TaOEt/O_3	73 nm	2.27 ± 0.03	0.2	
100 × [6 × 0.5/1.0 s, TaOEt/O_3 + 1 × 0.5/1.5 s, $ZrCl_4$/O_3] + 6 × 0.5/1.0 s, TaOEt/O_3	27-32 nm	2.224 ± 0.002	0.2	
1500 × 0.5/1.0/1.5 s, TaOEt/$ZrCl_4$/O_3	100-113 nm	2.52 ± 0.05	0.8	12.8 ± 0.2 Ta 16.7 ± 0.3 Zr 0.2 ± 0.1 Cl
280 × 0.5/1.0/1.5 s, TaOEt/$ZrCl_4$/O_3-p.	24-30 nm	2.203 ± 0.004	0.8	
750 × 0.5/1.0 s, TaOEt/$ZrCl_4$	25-34 nm	2.113 ± 0.001	0.9	12.5 ± 0.4 Ta 15.7 ± 0.6 Zr 4.6 ± 0.4 Cl
2 × 0.5/1.5 s, $ZrCl_4$/O_3 + 50 × [4 × 0.5/1.0/1.5 s, TaOEt/$ZrCl_4$/O_3] + 2 × 0.5/1.5 s, $ZrCl_4$/O_3	20-30 nm	2.186 ± 0.004	1.6	
250 × [5 × 0.5/1.5 s, $ZrCl_4$/O_3 + 1 × 0.5/1.5/0.5 s, $ZrCl_4$/O_3/TaOEt] + 6 × 0.5/1.5 s, $ZrCl_4$/O_3	120 nm	2.27 ± 0.03	7.8	

assuming a density of 5 g/cm^3 for ZrO_2. Surface morphology was monitored using the same SEM apparatus. The composition profile in selected as-deposited and annealed samples was determined by time-of-flight elastic recoil detection analysis (ToF-ERDA), using 35 MeV $^{127}I^{7+}$ beam. The measurement geometry was 15 ± 25° (scattering/detection angle 40°, incident angle 15° from sample surface). For depth scales, 5.0 g/cm^3 film density was considered.

For electrical measurements, Au/Pt/Ta_2O_5-ZrO_2/TiN/Si stacks were formed. Square shaped top electrodes with lateral dimensions of 100–300 μm were electron beam evaporated through a shadow mask. The electrodes consisted of 30 nm thick platinum layer in direct contact to Ta_2O_5-ZrO_2 film, followed by the topmost 30 nm thick Au layer. Electrical characterization of the prepared structures was performed using a Keithley 4200 Semiconductor Characterization System. During the measurement the top electrode was biased and the bottom TiN electrode was grounded.[66]

RESULTS AND DISCUSSION

Film growth and composition

In regard with the elemental composition, in a 33.5 ± 1.0 nm thick film as-deposited using 750 cycles consisting of sequential pulses of $Ta(OEt)_5$ and $ZrCl_4$ separated by purge periods, the

ToF-ERDA revealed 12.5±0.4 at.% Ta, 15.7±0.6 at.% Zr, 63.8 ± 1.7 at.% O, 2.5 ± 0.5 at.% H, 1.0 ± 0.2 at.% C, and 4.6 ± 0.4 at.% Cl (Fig. 1). In accord with EDX, the Zr:Ta cation ratio in this sample was 0.9. The amounts of metal cations in the film were almost equal, which may also be expected due to the equal amounts of the metal precursor pulses. After 30 min annealing in nitrogen at 800 °C, the elemental contents were 12.8 ± 0.4 at.% Ta, 14.5 ± 0.5 at.% Zr, 69.2 ± 1.4 at.% O, 2.3 ± 0.4 at.% H, 1.1 ± 0.2 at.% C, 0.2 ± 0.1 at.% Cl. One can see, that the atomic contents of the metals were the same, within the error limits, before and after heat-treatment. One can also see that the content of lighter and residual elements was not essentially affected by the annealing, except that of chlorine with the content noticeably decreasing from 4.6 to 0.2 at.%. Certain overlap visible in depth profiles of the film and substrate at the interface is due to the measurement technique. In heavy ion techniques, multiple scattering is essential issue, causing angular and energy broadening of the probing beam and detected particles detected after scattering or recoil processes. Because of multiple scattering and energy straggling, by energy loss for the particles, the depth resolution weakens deeper in the sample, especially in samples containing heavy elements like tantalum. In addition, issues related to the roughness of film surface and interfaces can interfere in the determination of the exact borderlines between distinct layers, especially considering the low incidence angle, 15°. Effects of multiple scattering and energy straggling are not corrected in the Figure 1.

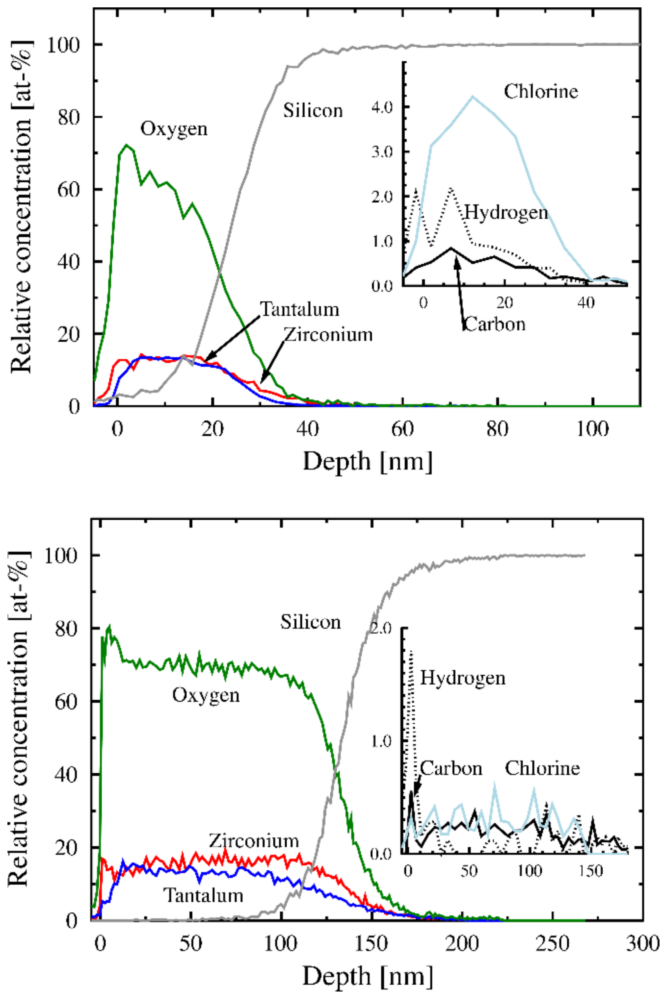

FIG. 1. Time-of-flight elastic recoil detection analysis results as elemental composition profiles from as-deposited films grown using 750 × 0.5-0.5-1.0-0.5 s long cycles for TaOEt-p.-$ZrCl_4$-p. pulse sequences (upper panel) and 1500 × 0.5-0.5-1.0-0.5 -1.5-0.5 s, TaOEt-p.-$ZrCl_4$-p.-O_3-p. cycles (lower panel).

Application of ozone did not noticeably influence the composition of the metal oxide films, in terms of the cation ratio. ToF-ERDA carried out on a 113 nm thick film deposited using 1500 cycles consisting of sequential pulses of $Ta(OEt)_5$, $ZrCl_4$, and O_3, separated by purge periods, contained 12.8 ± 0.2 at.% Ta, 16.7 ± 0.3 at.% Zr, 69.2 ± 1.4 at.% O, 2.3 ± 0.4 at.% H, 1.1 ± 0.2 at.% C, and 0.2 ± 0.1 at.% Cl (Fig. 1). In accord with the EDX analysis, although taken from a different location on the sample, the Zr:Ta cation ratio in this film was 0.83. One could see, that the application of ozone has not strongly affected the composition of the films, compared to the films grown using alternate pulsing of TaOEt and $ZrCl_4$ without ozone. The contents of hydrogen and carbon were not affected by the additional exposure to ozone. However, there was certain decrement in the content of chlorine detected, compared to those measured in the film deposited without ozone. This can plausibly be explained by the fact that the ozone was applied after the $ZrCl_4$ pulse, thus probably assisting in the completion of the oxidation of the Zr layer and more effective removal of chlorine species terminating the underlying tantalum zirconium oxide film.

The refractive index values measured by spectroscopic ellipsometry (Table I) were close to those commonly characterizing Ta_2O_5 and ZrO_2. No clear correlation between the refractive index and relative cation contents in the films was observed, which is plausibly due to the similarity of the refractive indexes of these materials. However, the values obtained are indicative of the formation of optically dense solid layers.

Fig. 2 demonstrates selected cross-sectional transmission electron microscopy images from an as-deposited film grown with the Ta_2O_5:ZrO_2 cycle ratio of 6:1 (Fig. 2, top panel), an annealed film grown with the Ta_2O_5:$TaZrO_x$ cycle ratio of 3:1 (Fig. 2, 2nd panel from top), an as-deposited films grown in exchange reactions between $Ta(OEt)_5$ and $ZrCl_4$ assisted with O_3 (Fig. 2, 3rd and 4th panels from top). Here the Ta_2O_5:$TaZrO_x$ cycle ratio 3:1 is used to denote ALD cycle sequences of 160 × [3 × 0.5-0.5-1.5-0.5 s, TaOEt-p.-O_3-p. + 1 × 0.5-0.5-0.5-0.5-1.5-0.5 s, TaOEt-p.-$ZrCl_4$-p.-O_3-p.], i.e. deposition of alternate layers of non-doped Ta_2O_5 and mixed Ta_2O_5:ZrO_2. One can see that the as-deposited layers are amorphous, uniform, smooth and with sharp interface with the underlying TiN. Also the image taken from an annealed sample represents an uniformly crystallized and well adhered region of the film. It is, however, to be noted, that the films often tended to be detached from the TiN, possibly due to the mismatch between elastic properties as well as the zirconate and titanium nitride lattice parameters, and differences in thermal expansion coefficients.

Regarding the film growth rate, the film deposited using 750 ALD cycles consisting of sequential pulses of $Ta(OEt)_5$ and $ZrCl_4$ separated by purge periods without ozone grew with the rate of 0.045 nm/cycle. The 113 and 21 nm thick films deposited using 1500 and 280 ALD cycles consisting of sequential pulses of $Ta(OEt)_5$, $ZrCl_4$, and O_3 grew with the rate of 0.075 nm/cycle. The growth rate per cycle has remarkably increased upon the application of ozone pulses. On the other hand, the additional ozone pulses have naturally increased the length of single ALD cycles, and, in this regard, the absolute growth rates for these three films remained similar, 0.017-0.018 nm/s. For comparison, reference Ta_2O_5 and ZrO_2 films grown from $Ta(OEt)_5$-O_3 and $ZrCl_4$-O_3 precursor systems, respectively, grew with rates 0.035 and 0.07 nm/cycle.[60]

The films with the Ta_2O_5:ZrO_2 cycle ratio of 6:1 were grown to different thicknesses using general cycle sequence $N \times [6 \times Ta_2O_5 + 1 \times ZrO_2] + 6 \times Ta_2O_5$. The thicknesses were 4.2 ± 0.1, 5.6 ± 0.2, 32.2 ± 0.4, and 106 nm for the N values of 6, 10, 100, and 300, respectively. One can see, that the film thickness increased, in practice, proportionally to the total number of the constituent oxide cycles. This was also expected as one of the characteristic features of a pulsed deposition process.

In a 106 nm thick film deposited using O_3 pulse after each metal precursor pulse with reduced relative amount of zirconium and with reduced relative amount of zirconium, i.e. with a cycle sequence $300 \times [6 \times Ta_2O_5 + 1 \times ZrO_2] + 6 \times Ta_2O_5$, the ToF-ERDA revealed 23.3 ± 0.2 at.% Ta, 7.4 ± 0.1 at.% Zr, 69.1 ± 0.9 at.% O, and. The amounts of carbon and chlorine were not detectable. One can see that the application of ozone pulses after each metal precursor pulse resulted in higher purity in terms of residual contamination, compared to the films deposited with ozone pulse applied only after the $ZrCl_4$ pulses. This was somewhat expected, because also in earlier reports on water-free ALD using surface reactions between metal precursors only,[55,56] the contents of residues have been relatively high. Annealing at 800 °C did not changed the composition of the film, as verified by ToF-ERDA, as they still contained 0.2 ± 0.1 at.% H. The fact that the hydrogen was not quite removed by anneling,

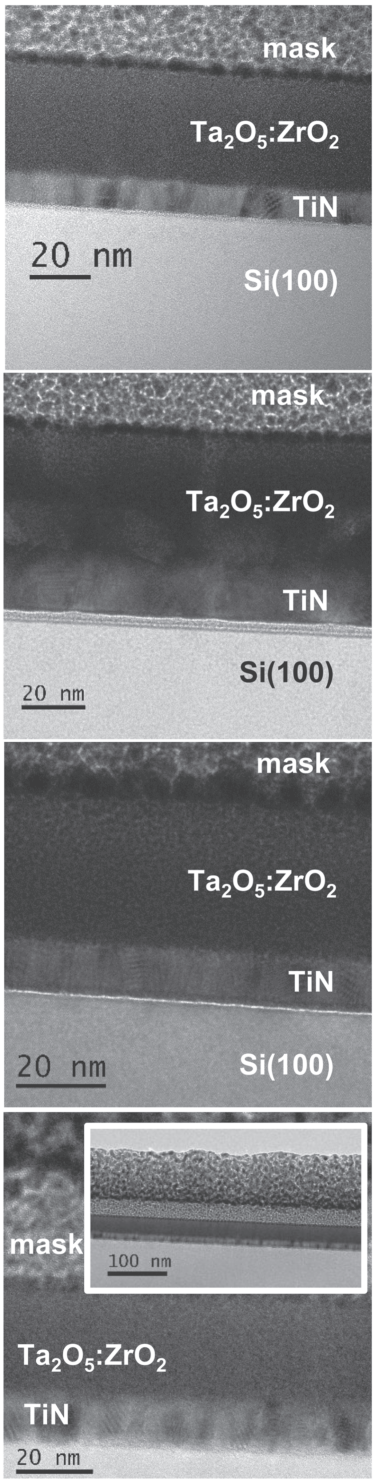

FIG. 2. Transmission electron microscopy images from a Ta_2O_5:ZrO_2 film as-deposited on TiN electrode using Ta_2O_5:ZrO_2 cycle ratio of 6:1 with cycle sequences of 100 × [6 × 0.5-0.5-1.0-0.5 s, TaOEt-p.-O_3-p. + 1 × 0.5-0.5-1.5-0.5 s, $ZrCl_4$-p.-O_3-p.] + 6 × 0.5-0.5-1.0-0.5 s, TaOEt-p.-O_3-p. (top panel); a film annealed on TiN and deposited using cycle sequence of 160 × [3 × 0.5-0.5-1.5-0.5 s, TaOEt-p.-O_3-p. + 1 × 0.5-0.5-0.5-0.5-1.5-0.5 s, TaOEt-p.-$ZrCl_4$-p.-O_3-p.] + 10 × 0.5-0.5-1.5-0.5 s, TaOEt-p.-O_3-p. (2nd panel from top); 750 × 0.5-0.5-1.0-0.5 s, TaOEt-p.-$ZrCl_4$-p. (3rd panel from top); and 2 × 0.5-0.5-1.5-0.5 s, $ZrCl_4$-p.-O_3-p. + 50 × [4 × 0.5-0.5-1.0-0.5-1.5-0.5 s, TaOEt-p.-$ZrCl_4$-p.-O_3-p.] + 2 × 0.5-0.5-1.5-0.5 s, $ZrCl_4$-p.-O_3-p. (bottom panel). The inset in the bottom panel shows a cross-section from the same sample in larger scale in order to illustrate the lateral uniformity of the film thickness.

may be explained by the probable diffusion of environmental water/hydrogen back into the material upon storage in the air.

It has been observed earlier that the thin films formed by the water-free ALD process tend to contain relatively high amounts of residual impurities compared to the films grown by ALD processes using water.[55] Also, the Ta_2O_5 films grown from $Ta(OC_2H_5)_5$ and $TaCl_5$[56] contained higher amounts of hydrogen and carbon compared to the Ta_2O_5 films grown from $Ta(OC_2H_5)_5$ and H_2O[67] or Ta_2O_5 films grown from $TaCl_5$ and H_2O.[68] The carbon impurities in tantalum oxide are found to be preferentially located in the neighborhood of the oxygen vacancies, and they reduce the oxygen-vacancy formation energy, which is predicted to have an influence on lowering the forming voltage.[69] Oxygen deficiency in Ta_2O_5 and its effect to the band gap energetics has been characterized thoroughly.[70]

Structural analysis

Ta_2O_5 films grown by ALD from $Ta(OC_2H_5)_5$ and H_2O or from $Ta(OC_2H_5)_5$ and $TaCl_5$ were all amorphous, as has also been observed in earlier works with the same process chemistries.[66,67] The Ta_2O_5 films not mixed with ZrO_2 or mixed with low amounts of ZrO_2 in the present study were crystallized upon annealing to the dominating hexagonal phase (Fig. 3, top panel) similarly to that observed in the earlier studies on crystallized Ta_2O_5 thin films.[67]

The Ta_2O_5 films doped with low amounts (Zr:Ta atomic ratio ca. 0.2) of zirconium (oxide) crystallized quite laboriously, showing only rather weak XRD peaks after 30 minutes annealing at 800 °C, whereas tantalum oxide grown without mixing it with zirconium oxide was crystallized quite intensely into the hexagonal δ-Ta_2O_5. This is consistent with results by Tewg *et al.*[71] reporting suppression of the crystallization of Ta_2O_5 with zirconium oxide doping.

The films deposited using equal amounts of sequential $Ta(OEt)_5$ and $ZrCl_4$ pulses, separated either only by purge times or additionally by intermediate ozone pulses, were also amorphous in the as-deposited state. Such films contained approximately equal amounts of zirconium and tantalum, and were crystallized after annealing at 800 °C, quite independently of the film thickness (Fig. 3, middle panel). The main phase recognized was evidently $TaZr_{2.75}O_8$ (PDF-042-0060) which also seems to be the only defined ternary tantalum zirconium oxide phase. Some minor peaks could be attributed to the reflections from ZrO_2, in addition.

The films with zirconium to tantalum atomic ratio above 1.0-1.6, dominantly consisting of ZrO_2, became crystallized already in the as-deposited state (Fig. 3, bottom panel), to structures characteristic of stable and metastable zirconium oxide polymorphs. Notably, the phase composition in terms of the major contributing polymorphs was not altered after annealing. The degree of crystallization, however, was enhanced, as decided on the basis of the intensity of the reflection peaks increasing upon the annealing.

Undoped ZrO_2 films grown by ALD from $ZrCl_4$ and O_3 were strongly polycrystalline with a rather large contribution from metastable cubic or tetragonal phase, similarly to that observed before.[60] Unambiguous and exact determination of phase composition of the ZrO_2 films containing amounts of additive tantalum relatively low compared to zirconium is not straighforward. One could see, that the films can be regarded as polycrystalline mixtures of stable monoclinic polymorph with characteristic -111 and 111 reflections at 28.3 and 31.8°, respectively, and metastable polymorphs with the most characteristic peak at ca. 30.3°. It occurred, however, quite complicated to attribute this peak distinctively to 111 cubic, 101 tetragonal or 101 orthorhombic phase reflections. Due to the width of the peaks as well as possible shifts in the peak positions caused by internal stresses, also the appearance of the reflections at larger angles did not make the phase determination much more feasible. There appeared, however, a few minor peaks attributable only to the orthorhombic polymorph, such as 211, 220, 212, and 113 reflections at 43.5, 51.0, 53.4 and 58.6°, respectively (not shown). It is to be noted that the orthorhombic phase (PDF Card 037-1413) is metastable under atmospheric pressure and reverts to the monoclinic phase on heating above 300 °C. It seems that the orthorhombic phase was the first one trying to form upon deposition and most of it was transformed into the monoclinic during the film growth already. There were also some peaks attributable only to the monoclinic polymorph. Somewhat surprisingly, there were no obvious peaks attributable only to the otherwise more-known and more often considered cubic phase.

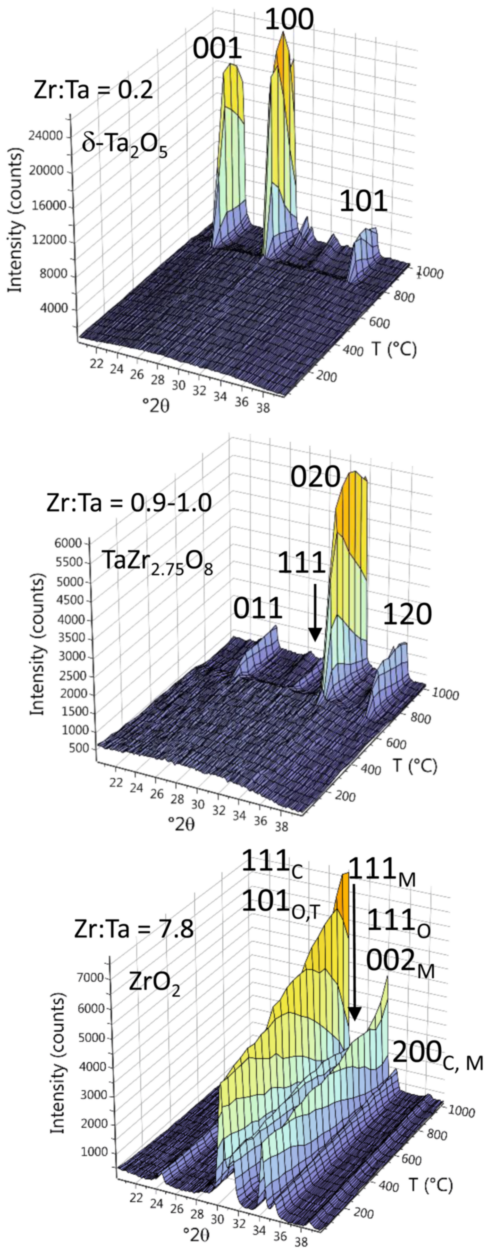

FIG. 3. High-temperature X-ray diffractograms from Ta_2O_5:ZrO_2 films deposited using cycle sequences 250 × [5 × 0.5-0.5-1.0-0.5 s, TaOEt-p.-O_3-p. + 1 × 0.5-0.5-1.0-0.5-1.5-0.5 s, TaOEt-p.-$ZrCl_4$-p.-O_3-p.] + 5 × 0.5-0.5-1.0-0.5 s, TaOEt-p.-O_3-p. (top panel), 1500 × 0.5-0.5-1.0-0.5 s, TaOEt-p.-$ZrCl_4$-p. (middle panel), and 250 × [5 × 0.5-0.5-1.5-0.5 s, $ZrCl_4$-p.-O_3-p. + 1 × 0.5-0.5-0.5-0.5- s, $ZrCl_4$-p.-O_3-p.-TaOEt] + 6 × 0.5-0.5-1.0-0.5 s, $ZrCl_4$-p.-O_3-p. (bottom panel). The film thicknesses were 73 nm, 42 nm, and 120 nm, respectively. Zr:Ta atomic ratios measured by EDX, dominant crystallographic phases identified, and Miller indexes assigned to the main reflections from the dominant phases are indicated by labels.

RESISTIVE SWITCHING CHARACTERISTICS

Resistive switching characteristics were studied by repeatedly forming and resetting conduction current paths through the oxide layer by applying external voltages of alternating polarity on TiN/Ta_2O_5:ZrO_2/Pt stacks. All the Ta_2O_5:ZrO_2 films deposited in this study demonstrated resistive switching characteristics when measured in as-deposited and mostly amorphous states. Resistive switching could not be observed after increment of long-range ordering, i.e. crystallization, of the

films by annealing at 800 °C for 10-30 min in N_2. Figure 4 depicts resistive switching characteristics of the as-deposited 20-35 nm thick Ta_2O_5:ZrO_2 films.

The film containing zirconium in the amounts below the detection level of EDX required rather high electroforming voltages up to 4 V to the ca. 30 nm thick film (Fig. 4, top panel). The range of the set/reset voltages required for switching between low and high resistance states remained between -2 and +2.5 V, approximately. The window between low and high resistance states was not very stable against the increasing number of voltage cycles, and reached two orders of magnitude in the current density scale, at maximum. These films were amorphous in the as-deposited state, and were crystallized after annealing into hexagonal Ta_2O_5 phase as described above.

The tantalum oxide films containing low, but still measurable amounts of zirconium (0.2 at. %) exhibited the most clearly defined resistive switching memory windows ranging over 4 orders of magnitude in the current scale (Fig. 4, 2nd panel from top). The forming voltage was at around 2.5 V in the ca. 30 nm thick film and did not noticeably exceed the working voltage in the filament setting current regime. Such kinds of films were amorphous in the as-deposited state, and crystallized relatively weakly after annealing at 800 °C, revealing only one rather low diffraction peak attributable to the 011 reflection from hexagonal δ-Ta_2O_5 as described above.

The films grown using direct surface reaction cycles between only $Ta(OEt)_5$ and $ZrCl_4$ (Fig. 4, 3rd panel from top), as well as those grown completing the same reaction cycles with O_3 pulse (Fig. 4, 4th panel from top) also demonstrated resistive switching behavior. In these films, the contents of tantalum and zirconium were comparable, i.e. the tantalum to zirconium cation ratios were 0.9 and 0.8, respectively, measured by EDX. One could see, however, that the stability of the switching loops was somewhat worsened again, compared to the loops recorded from the film with the Zr:Ta atomic ratio of 0.2. The width of the memory window in terms of the difference between low and high resistance states was noticeably more scattered during the subsequent voltage cycles, between one to two orders of magnitude in the current scale. The forming voltage for the ca. 30 nm thick films was at around 2 V, being comparable to the set/reset switching voltages. These films were, similarly to the others, amorphous in the as-deposited states. These films were crystallized rather intensely upon annealing, possessing polycrystalline nature and contained the $TaZr_{2.75}O_8$ ternary phase.

In the films containing ZrO_2 in amounts exceeding that of Ta_2O_5 (Fig. 4, bottom panel), the resistive switching became rather unstable in terms of the width of the gap between the low and high resistance states. For ca. 20 nm thick film, the difference between these states could vary between two and four orders of magnitude.

The annealing procedure resulted in the crystal growth in the initially highly disordered, i.e. amorphous, films. The annealing also suppressed the appearance of the resistive switching effect, regardless of the chemical composition of the films. The films measured after annealing demonstrated rather high leakage currents already in their virgin states, i.e. were conductive and thus already in the low resistance states. Electroforming of filamentary current channels occurred impossible. This may plausibly arise from the polycrystalline nature of the films, with defective and electronically leaky grain boundary networks extending from bottom to top electrodes. In addition, TEM studies revealed, in several cases, also possible intermixing of the TiN and metal oxide films as well as delamination of the oxide layers from the electrode (not shown). These distortions in layered metal-oxide-metal stacks have evidently caused permanent short circuits between the bottom and top electrodes.

The series of metal-dielectric-metal stacks formed in this study comprised the first resistive switching results on ALD Ta_2O_5-ZrO_2 films grown to thicknesses exceeding 20 nm and with variable chemical composition. It is complicated and yet premature to directly compare their performance to the behavior of reference stacks described in the literature. It has been emphasized, that electroforming step voltages, if considerably higher than that of switching voltage, need to be reduced in order to produce technologically relevant ReRAM devices.[17] Also, low operation voltages are desirable for sub-20 nm CMOS devices.[30] It has also been stated, that the electroforming conditions may strongly depend on the dimensions of the sample, especially, on the switching material thickness.[17] Tantalum oxide based ReRAM structures have mostly been grown by physical vapor deposition to thicknesses ranging from 5-20 nm, and, partially, using nonstoichiometric targets in relation to the pentoxide, as a feature related to the deposition process parameters.

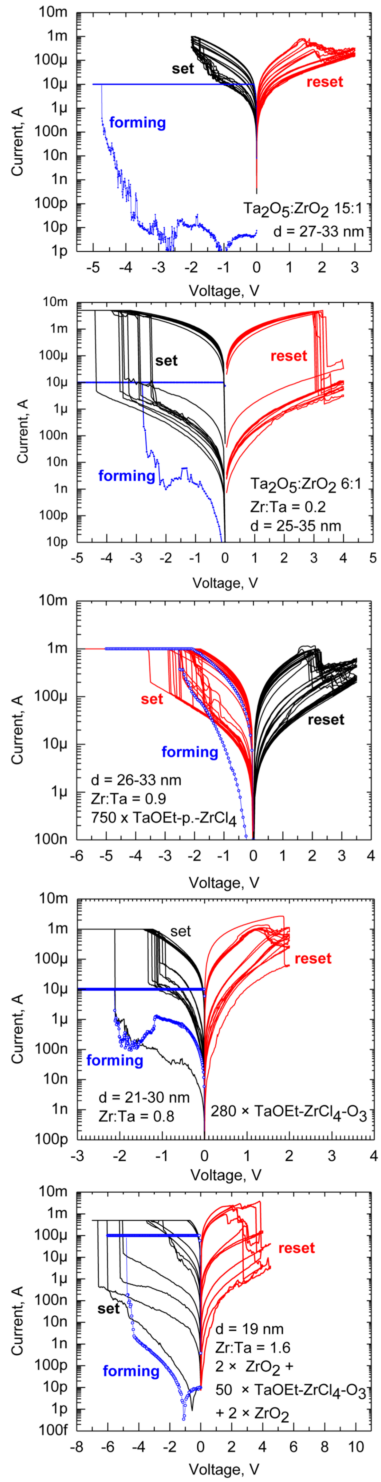

FIG. 4. Resistive switching current-voltage loops from Ta_2O_5:ZrO_2 films grown using cycle sequences of 40× [15 × 0.5-0.5-1.5-0.5 s, TaOEt-p.-O_3-p. + 1 × 0.5-0.5-0.5-0.5-1.5-0.5 s, TaOEt-p.-$ZrCl_4$-p.-O_3-p.] + 15 × 0.5-0.5-1.5-0.5 s, TaOEt-p.-O_3-p. (top panel); 100 × [6 × 0.5-0.5-1.0-0.5 s, TaOEt-p.-O_3-p. + 1 × 0.5-0.5-1.5-0.5 s, $ZrCl_4$-p.-O_3-p.] + 6 × 0.5-0.5-1.0-0.5 s, TaOEt-p.-O_3-p. (2nd panel from top); 750 × 0.5-0.5-1.0-0.5 s, TaOEt-p.-$ZrCl_4$-p. (3rd panel from top); 280 × 0.5-0.5-1.0-0.5-1.5-0.5 s, TaOEt-p.-$ZrCl_4$-p.-O_3-p. (the 4th panel), and 2 × 0.5-0.5-1.5-0.5 s, $ZrCl_4$-p.-O_3-p. + 50 × [4 × 0.5-0.5-1.0-0.5-1.5-0.5 s, TaOEt-p.-$ZrCl_4$-p.-O_3-p.]+ 2 × 0.5-0.5-1.5-0.5 s, $ZrCl_4$-p.-O_3-p. (bottom panel). Film thicknesses, Zr:Ta atomic ratios measured by EDX, and growth cycle sequences expressed either in Ta_2O_5:ZrO_2 cycle ratios or amounts of cycles consisting of subsequent TaOEt, $ZrCl_4$ and O_3 pulses are given by labels.

For instance, Pt/TaO_x/HfN_x structures with 20 nm thick TaO_x films were made by Zhou and Zhai[30] by magnetron sputtering TaO_2 (purity 99.9%) ceramic targets and using a substrate temperature of 200 °C. In these stacks, the forming voltage was −3.7 V, larger than the set voltage, -2 V, between the high and low resistance states, and also the initial leakage current was much smaller compared with the leakage current in the high resistance state after forming, rather similarly to the behavior observed in our samples.

In another study by Prakash *et al.*,[30] W/TaO_x/W and/or Pt/TaO_x/Pt structures were constructed or referred to, with thin TaO_x films comprising, e.g. Ta_2O_{5-x} insulating layer and a TaO_{2-x} base layer, with 6-30 nm total thicknesses for the TaO_x films. All the devices with different sizes from 50 × 50 μm^2 to 30 × 30 nm^2 showed self-compliant bipolar switching with small set/reset voltages of −1.0/2.0 V. The switching currents for, e.g., 50 × 50 μm^2 and 30 × 30 nm^2 devices were >200 μA and 40 μA, respectively.

Furthermore, Ta/TaO_x/Pt stacks have been formed by Yang *et al.*,[26] containing 7-18 nm thick $TaO_{1.7}$ layers sputtered from a target with nominal stoichiometry of TaO_2. These devices could be switched at rather low voltages, and the switching current was less than 100 μA insensitively to the device area. The forming voltage for the first set operation was ca. 0.8 V, only slightly larger than the subsequent normal set voltage, 0.6 V. Window between high and low resistance state currents ranged from 10 to 100 μA. Regarding the downscaling of the functional layer thicknesses, Park *et al.*[29] have described TiN/Ta_2O_5/Ta/TaN based switching stacks containing only 0.5-2.0 nm thick Ta_2O_5 layers grown by ALD with the active memory cell diameter of 28 nm. All the devices showed high resistance values of ~10^4–10^6 Ω, displaying bipolar resistance switching behavior after the electroforming steps. All the devices showed a limited maximum current of ~100 μA at −1.0 V.

In addition, Ta/Ta_2O_5/TiN stacks with lateral size of 100 nm x 100 nm have been described [Chen *et al.*[28]], containing amorphous 6 nm thick Ta_2O_5 layers grown by ALD at 250 °C using $TaCl_5$ and H_2O as precursors. The switching current was fixed at 50 μA. The devices were effectively set and reset using pulse amplitudes lower than 1.5 V.

It has been established, that the successful development of ReRAM structures is dependent on the possibility to scale down the switching material layer thickness together with the concurrent decrement of the filament forming voltage to the level comparable to that of the operational set-reset voltages. This research direction would be most appropriate after the determination of the layer composition optimized in terms of both structural and electrical stability. In the present work, the analysis results on Ta_2O_5 films doped with low amounts of ZrO_2 were indicative of the most stable structural and resistive behavior. Further studies on such material layers can be planned accordingly.

SUMMARY

Tantalum zirconium oxide mixture films were grown to thicknesses ranging from 20 to 100 nm by atomic layer deposition of either alternating layers of Ta_2O_5 and ZrO_2 from $Ta(OC_2H_5)_5$, $ZrCl_4$, and O_3, or using direct surface reactions between the same metal precursors. The cation ratio in the films could be varied with the sequence and ratio between deposition cycles of the single constituent oxides. Ozone pulses were optionally applied either after both $Ta(OC_2H_5)_5$ and $ZrCl_4$, or only after the $ZrCl_4$ pulses, in order to complete the oxidation reactions. Application of ozone assisted in the decrement of chlorine residues, as well as in the enhancement of the film growth rate.

Resistive switching properties were recorded in all the films in their as-deposited states, whereas annealing procedure at 800 °C, although crystallizing the films, occurred destructive regarding the switching behaviour. The major factor affecting the resistive switching properties the in as-deposited state was, evidently, the zirconium to tantalum cation ratio. Ta_2O_5 doped moderately with ZrO_2, i.e. with Zr:Ta ratio of 0.2, occurred the most hard to crystallize. At the same time, this material exhibited the most well defined resistive switching properties with the most symmetric and stable current-voltage loops against the repetitive switching voltage cycle. The films containing lower and higher amounts of Zr crystallized relatively strongly, i.e. more easily, but exhibited either more scattered or narrower current-voltage loops already in the as-deposited states.

The films containing Zr and Ta cations in the ratios close to unity were crystallized quite intensely upon annealing, indicating the formation of ternary $TaZr_{2.75}O_8$ phase. The films containing relatively

low amounts of Zr were crystallized as hexagonal Ta_2O_5. The films containing higher amounts of Zr were dominantly crystallized into metastable cubic/tetragonal or orthorhombic ZrO_2 phases. The annealed and crystallized films did not exhibit resistive switching probably due to the dominant grain boundary conduction and/or destruction/delamination of the electrode-metal oxide-electrode stack. The fact that good device switching results are achieved with smooth amorphous films can be a clear advantage for applications, as low-roughness amorphous ALD films are easier to integrate than polycrystalline films. Further investigations are to be directed towards lowering the electroforming voltage, decreasing film thickness and studying the possibilities to densify the films by adjustment of appropriate annealing parameters.

ACKNOWLEDGMENTS

The study was partially supported by the Finnish Centre of Excellence in Atomic Layer Deposition (284623), Estonian Academy of Science (SLTFYPROF), Estonian Research Agency (IUT2-24), Slovak Grant Agency (APVV-0560-14 and VEGA 2/0138/14). We thank the Electron Microscopy Unit of the Institute of Biotechnology at the University of Helsinki for instrument access and staff support.

[1] B. Samaranch, P. R. de la Piscina, G. Clet, M. Houalla, P. Gélin, and N. Homs, "Synthesis and characterization of Ta_2O_5-ZrO_2 systems: Structure, surface acidity, and catalytic properties," Chem. Mater. **19**, 1445–1451 (2007).
[2] M. A. Ewaida, M. M. Abou Sekkina, E. M. Ebrahim, and A. A. Al-Adawy, "Novel studies on the thermoelectro-mechanical properties of tantala doped zirconia ceramics," Polymer Degradation and Stability **21**, 227–235 (1988).
[3] S. Raghavan and M. J. Mayo, "The hot corrosion resistance of 20 mol% $YTaO_4$ stabilized tetragonal zirconia and 14 mol% Ta_2O_5 stabilized orthorhombic zirconia for thermal barrier coating applications," Surf. Coat. Technol. **160**, 187–196 (2002).
[4] M. H. Habibi, S. Yang, and S. M. Guo, "Phase stability and hot corrosion behavior of ZrO_2–Ta_2O_5 compound in Na_2SO_4–V_2O_5 mixtures at elevated temperatures," Ceram. Int. **40**, 4077–4083 (2014).
[5] M. Höftberger and G. Gritzner, "Niobia and tantala codoped orthorhombic zirconia ceramics," Scripta Metall. Materialia **32**, 1237–1241 (1995).
[6] A. Pissenberger and G. Gritzner, "Preparation and properties of niobia- and tantala-doped orthorhombic zirconia," J. Mater. Sci. Lett. **14**, 1580–1582 (1995).
[7] A. Taylor, R. E. Alonso, L. A. Errico, A. López-García, P. de la Presa, A. Svane, and N. E. Christensen, "Structural, electronic, and hyperfine properties of pure and Ta-doped m-ZrO_2," Phys. Rev. B **85**, 155202 (2012).
[8] J. C. Ray, A. B. Panda, and P. Pramanik, "Chemical synthesis of nanocrystals of tantalum ion-doped tetragonal zirconia," Mater. Lett. **53**, 145–150 (2002).
[9] C. Zheng and A. R. West, "Compound and solid-solution formation, phase equilibria and electrical properties in the ceramic system ZrO_2-La_2O_3-Ta_2O_5," J. Mater. Chem. **1**, 163–167 (1991).
[10] R. J. Cava and J. J. Krajewski, "Dielectric properties of Ta_2O_5–ZrO_2 polycrystalline ceramics," J. Appl. Phys. **83**(3), 1613–1616 (1998).
[11] C. H. Kim, "Synthesis of $ZrTiO_4$ and $Ta_2Zr_6O_{17}$ films by composition-combinatorial approach through surface sol-gel method and their dielectric properties," Bull. Korean Chem. Soc. **28**, 1463–1466 (2007).
[12] W. Luo, Y. Kuo, and W. Kuo, "Dielectric relaxation and breakdown detection of doped tantalum oxide high-k thin films," IEEE Transactions on Device and Materials Reliability **4**, 488–494 (2004).
[13] T. V. Rajesh, M. Kumar, C. J. Choi, E. Fortunato, S. Uthanna, and S. V. J. Chandra, "Zirconium oxide mixed tantalum oxide high-k gate dielectric films for metal-oxide-semiconductor (MOS) devices," Eur. J. Adv. Eng. Technol. **2**, 9–15 (2015), www.ejaet.com ISSN: 2394-658X.
[14] J.-Y. Tewg, Y. Kuo, J. Lu, and B. W. Schueler, "Electrical and physical characterization of zirconium-doped tantalum oxide thin films," J. Electrochem. Society **151**, F59–F67 (2004).
[15] J. Lu, Y. Kuo, J.-Y. Tewg, and B. Schueler, "Effects of the TaN_x interface layer on doped tantalum oxide high-k films," Vacuum **74**, 539–547 (2004).
[16] R. Waser and M. Aono, "Nanoionics-based resistive switching memories," Nature Mater. **6**, 833–840 (2007).
[17] A. Prakash, D. Jana, and S. Maikap, "TaO_x-based resistive switching memories: Prospective and challenges," Nanoscale Res. Lett. **8**, 418 (2013), http://www.nanoscalereslett.com/content/8/1/418.
[18] D. S. Jeong, R. Thomas, R. S. Katiyar, J. F. Scott, H. Kohlstedt, A. Petraru, and C. S. Hwang, "Emerging memories: Resistive switching mechanisms and current status," Rep. Prog. Phys. **75**, 076502 (2012).
[19] A. Wedig, M. Luebben, D.-Y. Cho, M. Moors, K. Skaja, V. Rana, T. Hasegawa, K. K. Adepalli, B. Yildiz, R. Waser, and I. Valov, "Nanoscale cation motion in TaO_x, HfO_x and TiO_x memristive systems," Nature Nanotech. **11**, 67–74 (2016).
[20] G. Bersuker and D. Gilmer, Metal oxide resistive random access memory (RRAM) technology, in: *Advances in Non-Volatile Memory and Storage Technology*, Ed.: Y. Nishi, Woodhead Publishing (2014), pp. 288–340.
[21] U. Celano, L. Goux, A. Belmonte, K. Opsomer, A. Franquet, A. Schulze, C. Detavernier, O. Richard, H. Bender, M. Jurczak, and W. Vandervorst, "Three-dimensional observation of the conductive filament in nanoscaled resistive memory devices," Nano Lett. **14**, 2401–2406 (2014).
[22] J. J. Yang, D. B. Strukov, and D. R. Stewart, "Memristive devices for computing," Nature Nanotech. **8**, 13–24 (2013).
[23] M.-J. Lee, C. B. Lee, D. Lee, S. R. Lee, M. Chang, J. H. Hur, Y.-B. Kim, C.-J. Kim, D. H. Seo, S. Seo, U.-I. Chung, I.-K. Yoo, and K. Kim, "A fast, high-endurance and scalable non-volatile memory device made from asymmetric Ta_2O_{5-x}/TaO_{2-x} bilayer structures," Nature Mater. **10**, 625–630 (2011).

[24] K. M. Kim, S. R. Lee, S. Kim, M. Chang, and C. S. Hwang, "Self-limited switching in Ta_2O_5/TaO_x memristors exhibiting uniform multilevel changes in resistance," Adv. Funct. Mater. **25**, 1527–1534 (2015).
[25] G.-S. Park, Y. B. Kim, S. Y. Park, X. S. Li, S. Heo, M.-J. Lee, M. Chang, J. H. Kwon, M. Kim, U.-I. Chung, R. Dittmann, R. Waser, and K. Kim, "In situ observation of fiamentary conducting channels in an asymmetric Ta_2O_{5-x}/TaO_{2-x} bilayer structure," Nature Comm. **4**, 1 (2013).
[26] J. J. Yang, M.-X. Zhang, J. P. Strachan, F. Miao, M. D. Pickett, R. D. Kelley, G. Medeiros-Ribeiro, and R. S. Williams, "High switching endurance in TaO_x memristive devices," Appl. Phys. Lett. **97**, 232102 (2010).
[27] Y. Yang, S. Choi, and W. Lu, "Oxide heterostructure resistive memory," Nano Lett. **13**, 2908–2915 (2013).
[28] C. Y. Chen, L. Goux, A. Fantini, S. Clima, R. Degraeve, A. Redolfi, Y. Y. Chen, G. Groeseneken, and M. Jurczak, "Endurance degradation mechanisms in TiN\Ta_2O_5\Ta resistive random-access memory cells," Applied Physics Letters **106**, 053501 (2015).
[29] T. H. Park, S. J. Song, H. J. Kim, S. G. Kim, S. Chung, B. Yong Kim, K. J. Lee, K. M. Kim, B. J. Choi, and C. S. Hwang, "Thickness effect of ultra-thin Ta_2O_5 resistance switching layer in 28 nm-diameter memory cell," Sci. Rep. **5**, 15965 (2015).
[30] Q. Zhou and J. Zhai, "Resistive switching characteristics of $Pt/TaO_x/HfN_x$ structure and its performance improvement," AIP Adv. **3**, 032102 (2013).
[31] S. Z. Rahaman, S. Maikap, T.-C. Tien, H.-Y. Lee, W.-S. Chen, F. T. Chen, M.-J. Kao, and M.-J. Tsai, "Excellent resistive memory characteristics and switching mechanism using a Ti nanolayer at the Cu/TaO_x interface," Nanoscale Res. Lett. **7**, 345 (2012), http://www.nanoscalereslett.com/content/7/1/345.
[32] R. J. Bondi and M. J. Marinella, "Oxidation state and interfacial effects on oxygen vacancies in tantalum pentoxide," J. Appl. Phys. **117**, 085308 (2015).
[33] M. Vos, P. L. Grande, S. K. Nandi, D. K. Venkatachalam, and R. G. Elliman, "A high-energy electron scattering study of the electronic structure and elemental composition of O-implanted Ta films used for the fabrication of memristor devices," J. Appl. Phys. **114**, 073508 (2013).
[34] N. Ge, M.-X. Zhang, L. Zhang, J. J. Yang, Z. Li, and R. S. Williams, "Electrode-material dependent switching in TaO_x memristors," Semicond. Sci. Technol. **29**, 104003 (2014).
[35] D. Panda and T.-Y. Tseng, "Growth, dielectric properties, and memory device applications of ZrO_2 thin films," Thin Solid Films **531**, 1–20 (2013).
[36] J. Lee, M. Jo, D.-j. Seong, J. Shin, and H. Hwang, "Materials and process aspect of cross-point RRAM (invited)," Microel. Eng. **88**, 1113–1118 (2011).
[37] Q. Liu, W. Guan, S. Long, R. Jia, M. Liu, and J. Chen, "Resistive switching memory effect in ZrO_2 films with Zr^+ implanted," Appl. Phys. Lett. **92**, 012117 (2008).
[38] M. N. Awais, N. M. Muhammad, D. Navaneethan, H. C. Kim, J. Jo, and K. H. Choi, "Fabrication of ZrO_2 layer through electrohydrodynamic atomization for the printed resistive switch (memristor)," Microel. Eng. **103**, 167–172 (2013).
[39] K.-H. Choi, N. Duraisamy, M. N. Awais, N. M. Muhammad, H.-C. Kim, and J. Jo, "Investigation on switching behavior of ZrO_2 thin film for memory device applications," Mater. Sci. Semicond. Processing **16**, 1285–1291 (2013).
[40] P. Parreira, S. McVitie, and D. A. MacLaren, "Resistive switching in ZrO_2 films: Physical mechanism for filament formation and dissolution," J. Phys.: Conf. Ser. **522**, 012045 (2014).
[41] P. Parreira, G. W. Paterson, S. McVitie, and D. A. MacLaren, "Stability, bistability and instability of amorphous ZrO_2 resistive memory devices," J. Phys. D: Appl. Phys. **49**, 095111 (2016).
[42] C.-H. Lai, C.-Y. Liu, and H. Yang, "Bipolar resistance switching characteristics in zirconium oxide," Ferroelectrics **457**, 146–152 (2013).
[43] M.-C. Wu, W.-Y. Jang, C.-H. Lin, and T.-Y. Tseng, "A study on low-power, nanosecond operation and multilevel bipolar resistance switching in $Ti/ZrO_2/Pt$ nonvolatile memory with 1T1R architecture," Semicond. Sci. Technol. **27**, 065010 (2012).
[44] H. Xie, Q. Liu, Y. Li, H. Lv, M. Wang, K. Zhang, S. Long, S. Liu, and M. Liu, "Effect of low constant current stress treatment on the performance of the $Cu/ZrO_2/Pt$ resistive switching device," Semicond. Sci. Technol. **27**, 105007 (2012).
[45] T.-L. Tsai, T.-H. Ho, and T.-Y. Tseng, "Unipolar resistive switching behaviors and mechanisms in an annealed $Ni/ZrO_2/TaN$ memory device," J. Phys. D: Appl. Phys. **48**, 035108 (2015).
[46] Q. Liu, S. Long, W. Wang, Q. Zuo, S. Zhang, J. Chen, and M. Liu, "Improvement of resistive switching properties in ZrO_2-based ReRAM with implanted Ti ions," IEEE Electr. Dev. Lett. **30**, 1299–1301 (2009).
[47] Q. Liu, S. Long, W. Wang, S. Tanachutiwat, Y. Li, Q. Wang, M. Zhang, Z. Huo, J. Chen, and M. Liu, "Low-power and highly uniform switching in ZrO_2-based ReRAM with a Cu nanocrystal insertion layer," IEEE Elect. Dev. Lett. **31**, 1299–1301 (2010).
[48] B. Zeng, D. Xu, M. Tang, Y. Xiao, Y. Zhou, R. Xiong, Z. Li, and Y. Zhou, "Improvement of resistive switching performances via an amorphous ZrO_2 layer formation in TiO_2-based forming-free resistive random access memory," J. Appl. Phys. **116**, 124514 (2014).
[49] S.-Y. Wang, D.-Y. Lee, T.-Y. Huang, J.-W. Wu, and T.-Y. Tseng, "Controllable oxygen vacancies to enhance resistive switching performance in a ZrO_2-based RRAM with embedded Mo layer," Nanotechnology **21**, 495201 (2010).
[50] Y. Li, S. Long, H. Lv, Q. Liu, Y. Wang, S. Zhang, W. Lian, M. Wang, K. Zhang, H. Xie, S. Liu, and M. Liu, "Improvement of resistive switching characteristics in ZrO_2 film by embedding a thin TiO_x layer," Nanotechnology **22**, 254028 (2011).
[51] R. G. Elliman, M. S. Saleh, T.-H. Kim, D. K. Venkatachalam, K. Belay, S. Ruffell, P. Kurunczi, and J. England, "Application of ion-implantation for improved non-volatile resistive random access memory (ReRAM)," Nucl. Instr. Methods Phys. Res. B **307**, 98–101 (2013).
[52] R. D. Clark, "Emerging applications for high k materials in VLSI technology," Materials **7**, 2913–2944 (2014).
[53] K. V. Egorov, Yu. Yu. Lebedinskii, A. M. Markeev, and O. M. Orlov, "Full ALD Ta_2O_5-based stacks for resistive random access memory grown with *in vacuo* XPS monitoring," Appl. Surf. Sci. **356**, 454–459 (2015).
[54] K. Y. Ahn and L. Forbes, "Zirconium-doped tantalum oxide films," Patent No. US2007/0087563A1.

[55] M. Ritala, K. Kukli, A. Rahtu, P. I. Räisänen, M. Leskelä, T. Sajavaara, and J. Keinonen, "Atomic layer deposition of oxide thin films with metal alkoxides as oxygen sources," Science **288**, 319–321 (2000).
[56] K. Kukli, M. Ritala, and M. Leskelä, "Atomic layer deposition and chemical vapor deposition of tantalum oxide by successive and simultaneous pulsing of tantalum ethoxide and tantalum chloride," Chem. Mater. **12**, 1914–1920 (2000).
[57] K. Kukli, J. Ihanus, M. Ritala, and M. Leskelä, "Properties of Ta_2O_5-based dielectric nanolaminates deposited by atomic layer epitaxy," J. Electrochem. Soc. **144**, 300–306 (1997).
[58] I. Jõgi, K. Kukli, M. Ritala, M. Leskelä, J. Aarik, A. Aidla, and J. Lu, "Atomic layer deposition of high capacitance density Ta_2O_5–ZrO_2 based dielectrics for metal–insulator–metal structures," Microelectronic Engineering **87**, 144–149 (2010).
[59] H. Cho, K.-W. Park, C. H. Park, H. J. Cho, S.-J. Yeom, K. Hong, N.-J. Kwak, and J.-H. Ahn, "Abnormally enhanced dielectric constant in ZrO_2/Ta_2O_5 multi-laminate structures by metallic Ta formation," Materials Letters **154**, 148–151 (2015).
[60] K. Kukli, M. Kemell, J. Köykkä, K. Mizohata, M. Vehkamäki, M. Ritala, and M. Leskelä, "Atomic layer deposition of zirconium dioxide from zirconium tetrachloride and ozone," Thin Solid Films **589**, 597–604 (2015).
[61] I. Kärkkänen, A. Shkabko, M. Heikkilä, J. Niinistö, M. Ritala, M. Leskelä, S. Hoffmann-Eifert, and R. Waser, "Study of atomic layer deposited ZrO_2 and ZrO_2/TiO_2 films for resistive switching application," Phys. Status Solidi A **211**, 301–309 (2014).
[62] T. Suntola, "Atomic layer epitaxy," Thin Solid Films **216**, 84–89 (1992).
[63] M. Ylilammi and T. Ranta-aho, "Optical determination of the film thicknesses in multilayer thin film structures," Thin Solid Films **232**, 56–62 (1993).
[64] L. A. Giannuzzi, J. L. Drown, S. R. Brown, R. B. Irwin, and F. A. Stevie, "Applications of the FIB lift-out technique for TEM specimen preparation," Microsc. Res. Tech. **41**, 285–290 (1998).
[65] R. A. Waldo, *Microbeam Analysis* (San Francisco Press, San Francisco, CA, 1988), p. 310.
[66] B. Hudec, A. Paskaleva, P. Jančovič, J. Dérer, J. Fedor, A. Rosová, E. Dobročka, and K. Fröhlich, "Resistive switching in TiO_2-based metal–insulator–metal structures with Al_2O_3 barrier layer at the metal/dielectric interface," Thin Solid Films **563**, 10–14 (2014).
[67] K. Kukli, M. Ritala, and M. Leskelä, "Atomic layer epitaxy growth of tantalum oxide films from $Ta(OC_2H_5)_5$ and H_2O," J. Electrochem. Soc. **142**, 1670–1675 (1995).
[68] K. Kukli, M. Ritala, R. Matero, and M. Leskelä, "Influence of the atomic layer deposition parameters on the phase content of Ta_2O_5 films," J. Cryst. Growth **212**, 459–468 (2000).
[69] J.-Y. Kim, B. Magyari-Köpe, Y. Nishi, and J.-H. Ahn, "First-principles study of carbon impurity effects in the pseudo-hexagonal Ta_2O_5," Curr. Appl. Phys. **16**, 638–643 (2016).
[70] Y. R. Denny, T. Firmansyah, S. K. Oh, H. J. Kang, D.-S. Yang, S. Heo, J. Chung, and J. C. Lee, "Effect of oxygen deficiency on electronic properties and local structure of amorphous tantalum oxide thin films," Mater. Res. Bull. **82**, 1–6 (2016).
[71] J.-Y. Tewg, Y. Kuo, and J. Lu, "Suppression of crystallization of tantalum oxide thin film by doping with zirconium," Electrochem. Solid-State Lett. **8**, G27–G29 (2005).